AIAA JOURNAL
Vol. 39, No. 6, June 2001

Near-Field Entrainment in an Impulsively Started Turbulent Gas Jet

G. E. Cossali*
Università di Bergamo, Dalmine 24044, Bergamo, Italy
and
A. Coghe† and L. Araneo‡
Politecnico di Milano, 20156 Milan, Italy

The entrainment characteristics of an impulsively started gas jet injected into quiescent atmosphere was studied by means of two-dimensional visualizations and laser Doppler velocimetry. The focus was on near-field behavior, where the velocity profiles are not self-similar, unlike those far downstream, and the unsteady jet head structure plays a relevant role in the early jet development. In the investigated near-field region, direct measurements of the size of the unsteady leading jet structure shows that its length is larger than 12 nozzle diameters and grows linearly with time. The present analysis indicates that early in the near field the jet volume becomes larger than the injected one and suggests a possible mechanism for surrounding gas entrainment into the jet head, which differs significantly from the mechanism responsible for entrainment in the quasi-steady part of the jet. It follows that the frequently used model that assumes the head vortex growing due to the mass entrainment from the steady-state jet cone only should be modified when dealing with the initial part of the jet injection. A further result is that the attainment of the steady-state conditions is faster on the jet axis than at the edges, where the mixing mechanism requires longer times to reach equilibrium.

Nomenclature

D_0	=	nozzle diameter
I	=	gray level
$I(r, z)$	=	gray level of two-dimensional picture at position (r, z)
J	=	momentum flux
$L(z)$	=	jet width at distance z from the nozzle
M	=	momentum flux ratio
$\dot{m}$	=	mass flow rate
r	=	radial distance from the jet axis
U_c	=	axial velocity at jet centerline
V	=	jet volume
v	=	air velocity
z	=	axial distance from injector nozzle
α	=	unsteadiness parameter
η	=	$z/(J/\rho)^{1/4}$
μ	=	nondimensional mass flow ratio, $(\dot{m}_e + \dot{m}_0)/\dot{m}_0$
ξ	=	nondimensional distance from nozzle, $z/D_0(\rho_e/\rho_0)^{1/2}$
ρ	=	density

Subscripts

a	=	ambient
av	=	average
cm	=	center of mass
e	=	entrained
j	=	jet
p	=	partial
r	=	radial
th	=	threshold
tip	=	jet tip
z	=	axial
0	=	at nozzle exit

Received 20 January 2000; revision received 24 April 2000; accepted for publication 9 November 2000.

*Professor, via Marconi 5.
†Professor, Department of Energy, via La Masa 34.
‡Research Scientist, Department of Energy, via La Masa 34.

I. Introduction

In recent years, renewed interest has been focused on efficient schemes for gaseous fuel injection. This is a process that is of concern in many engineering applications, such as scramjet combustors, gas turbine combustion chambers, reciprocating internal combustion engines, and steady-state industrial-type burners. Other examples of gaseous jets of great practical interest are found in vertical/short takeoff and landing aircraft, the cooling of turbine blades, and chimney stacks exhausting smoke into a wind. Steady incompressible turbulent free jets have been studied quite extensively in the past, both theoretically and experimentally. Much is known about their properties, such as the velocity distribution, the growth of the jet cross-sectional area, mass entrainment, etc., as documented in the fairly extensive literature.[1–3] It has been found that in the fully developed region, for sufficiently high nozzle Reynolds numbers, the transverse velocity profiles become self-similar and the jet spreads linearly. Moreover, the momentum flux ratio $M = \rho_j U_j^2/\rho_a U_a^2$ is the parameter controlling the penetration of the steady jet in a crossflow or the mixing characteristics in a coflowing stream.[4]

Unsteady injection is imposed, in many situations, by the periodic nature of the governing process, for example, in reciprocating engines where direct injection of natural gas into the cylinder of a diesel engine is an attractive solution because of its potential to reduce pollutant emissions.[5] Early studies of unsteady injection[6–8] found that mixing is greatly enhanced by the use of unsteady or fully pulsed incompressible air jets, when compared with a steady jet. Pulsed injection of gaseous jets has been recently proposed[9] as a way to increase the penetration of the injectant in supersonic flows, such as those of scramjet combustors.

Much about the downstream jet development has been learned from experiments. It has been recently shown[10] that a turbulent jet impulsively injected at constant rate into a large quiescent chamber exhibits a self-similar configuration after the tip has traveled 15–20 nozzle diameters from the exit plane. The literature survey reported in Ref. 10 shows that scaling based on nozzle exit momentum flux and density ratio applies for a wide range of conditions if the opening transient is short compared to the duration of injection. The consistency of self-similar profiles obtained under different operating conditions was found by using the equivalent nozzle diameter (defined as the nozzle diameter multiplied by the square root of nozzle-to-chamber density ratio), which has been introduced in scaling steady-state turbulent jets. Also highly underexpanded jets

conform to the downstream self-similar behavior,[11] and a universal penetration law can be obtained by scaling data with the square root of the nozzle-to-chamber density ratio.

These results are in agreement with a theoretical analysis that assumes constant momentum discharge rate and the vortex ball model firstly suggested by Turner for a starting plume.[12] Many authors[5,10,13] refer to this model in the approximation developed by Abramovich and Solan[14] for the initial development of a submerged laminar round jet. They modeled the starting jet as consisting of a spherical ball followed by a quasi-steady-state jet region and assumed that the vortex ball is growing due to the mass entrainment from the steady-state jet only. In the early 1980s, this model was applied by Witze[13] to an impulsively started incompressible turbulent jet, whereas Kuo and Bracco[15] have shown by calculation when quasi-steady behavior can be assumed for transient jets and sprays. The same model has been recently applied to a direct injection natural gas engine, and the vortex ball model of jet penetration agreed well with the penetration data of an underexpanded jet.[5]

Note that the transient mixing of free sprays in confined flows, typical of automotive engines, has been frequently modeled as a quasi-steady gas jet, based on the similarity with a single-phase gas jet of high density penetrating into a low-density gaseous medium.[16] As an example, in a recent study[17] a penetration relationship has been derived under a quasi-steady-state assumption, which reduces to the form reported in Ref. 10 for transient turbulent gaseous jets, in the limiting case of infinitely fast evaporation. Following this type of approach, sprays have been frequently modeled as a mixture of fuel droplets and entrained air, which propagate in a conical shape at some fixed cone angle, and the details of the starting vortex are not taken into account.

A more complex picture of a subsonic transient jet has been derived by means of laser sheet illumination and photographic analysis,[18] but no quantitative data or useful models have been provided. A previous study,[19] performed by means of laser-induced fluorescence (LIF), revealed that the jet concentration distribution in intermittent gas jets was very similar to that of steady jets except in the head region, where a higher concentration was found.

The purpose of the work reported in this paper was to investigate the near-field zone (up to 20 nozzle diameters) of a subsonic transient turbulent jet impulsively injected at constant rate into a large quiescent chamber. The jet behavior in this region is not well known because most of the investigations on impulsively started gas jets were focused on the later development of this flow. Moreover, this is the region of interest for many technological applications, such as gas injection in internal combustion engines, cooling of turbine blades, etc.

II. Experimental Setup

The experimental setup comprised a constant volume cylindrical chamber (180-mm internal diameter), containing quiescent air at room pressure and temperature, equipped with four windows (100-mm diam), which allowed optical access for laser Doppler velocimetry (LDV) measurements and visualization. A single hole nozzle (3-mm diam) was positioned on the top of the cylindrical chamber. A tilting mechanism, onto which the injection system was mounted, allowed alignment of the jet axis with the chamber axis, following a trial-and-error procedure based on LDV measurements of the jet velocity profile under steady conditions. Misalignment of the jet axis can be estimated to be less than 2 mm at 60 mm, that is, about ± 2 deg, which introduces deterministic errors (bias) in measuring each velocity component of about 3% of the other component. Large bias may be expected in measuring the radial velocity close to the jet axis, where the axial component is much higher than the radial one. However, relatively small bias will arise in measuring the radial component far from the jet axis, where the radial component is comparable or larger than the axial one.

The nozzle was connected to a small (0.0012-m^3) settling chamber (Fig. 1), through a solenoid valve, and the pressure and temperature of the injected gas into the chamber were continuously monitored by a pressure transducer and a thermocouple. The nozzle was mounted on a flat disk (100-mm diam) to produce a wall

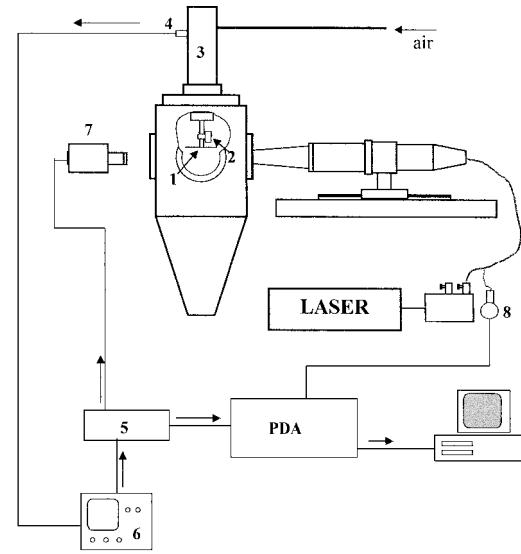

Fig. 1 Experimental setup: 1, nozzle; 2, solenoid valve; 3, settling chamber; 4, pressure transducer; 5, delay trigger; 6, oscilloscope; 7, CCD camera; and 8, photomultiplier.

condition at the nozzle exit. The settling chamber was connected through a pressure regulator to an air bottle to provide the desired injection pressure. The injection system was operated in the single injection mode. The valve was electrically operated and data acquisition [by a charge-coupled device (CCD) camera and LDV] was synchronized to the valve opening signal. The duration of injection was 30 ms, whereas the estimated valve opening transient was about 2 ms. A delay between the valve opening signal and the actual beginning of the injection exists, and it was measured to be equal to 10.1 ms, using the two-dimensional visualization setup described subsequently. The time origin was defined as the time at which the jet actually exits the nozzle, and the time variable will be referred to as after start of injection (ASI).

The average nozzle discharge coefficient, defined as the ratio between the actual injected mass and the nominal injected mass calculated from the injection pressure data (using the isoentropic flow assumption), was measured for steady conditions by direct measurement of the injected mass flow rate at different injection pressures. It was used to evaluate the instantaneous mass flow rate, in conjunction with measurement of instantaneous injection pressure. The instantaneous mass flow rate measured as described earlier varied between 5.93 and 5.50×10^{-4} kg/s during injection, and the corresponding Reynolds number varied between 1.26×10^4 and 1.36×10^4. The accuracy of this measurement was estimated to be better than 2%.

III. Measurement Techniques

Two laser-based techniques were used, namely, two-dimensional visualization and LDV. Both techniques required tracer particles, and micrometric silicon oil droplets were used for this purpose. The seeding system provided independent seeding of the jet gas and the chamber gas whenever it was necessary.

A. Visualization

An Ar-ion laser beam was spread into a sheet by a combination of spherical and cylindrical lenses and sent through the jet along its axis to produce a two-dimensional illumination of the gas jet. The average light sheet thickness in the jet region was less then 500 μm. A CCD camera (Flashcam PCO) with 1-μs time resolution captured the image. Image preprocessing comprised background noise subtraction and contrast enhancement. The spatial accuracy defining the absolute position of the single pixel on the images was on the order of 0.3 mm, which was considered sufficient for the present purposes, whereas the pixel resolution was about 0.1 mm. This technique was used to investigate tip penetration characteristics and jet structure by image analysis, as will be explained.

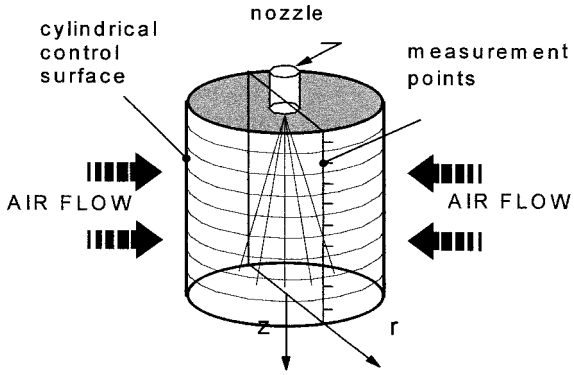

Fig. 2 Cylindrical control surface and the measuring points used to evaluate the air entrainment into the spray.

B. LDV

A dual-beam laser Doppler velocimeter (Dantec) was used, in the backscattering configuration, to measure the gas flowfield around and into the jet. The measuring system comprised a 5-W (nominal power) Ar-ion laser, a conventional fiber optic LDV transmitting unit with a 40-MHz Bragg cell for frequency shifting and directional sensitivity, and a front lens of 310-mm focal length. The nominal diameter of the geometrical control volume was 0.1 mm and its length 1 mm. A Dantec 58N10 particle Doppler analyzer (PDA) signal processor, with 1-μs time resolution, was used for data acquisition.

Data were collected over many injections and ensemble averaged. Radial and axial velocity components were measured (not simultaneously) in the region $-28 \le r \le +28$ mm and $30 \le z \le 65$ mm. To evaluate air entrainment into the jet, the radial velocity was also measured along two lines parallel to the jet axis at $r = \pm 20$ mm (Fig. 2). Data acquisition was triggered by the valve opening signal and performed for a 30-ms time window for each injection. The accuracy of velocity measurements is mainly due to statistical uncertainty, which depends on the velocity component, the measurement position, and the time ASI. The main quantitative results reported in the paper are those related to the entrainment obtained from radial velocities taken well outside the jet cone. In this case, the relative rms values were less than 10%, and the accuracy of the mean velocity was evaluated to be better than 2%.

IV. Results and Discussion

The procedure used to reduce the experimental data obtained by the mentioned techniques will be explained. The accuracy of the results will be also discussed, together with the main findings, and attempts will be made to extract physical meanings whenever possible.

A. Image Analysis

Laser sheet visualization of the jet evolution allowed the jet tip penetration to be measured and illustrated some interesting features of the phenomenon. Tip penetration relationships obtained by simplified models are often compared to experimental data to assess their validity. However, it is important to compare measurements and predictions relative to the same definition of jet tip. The tip arrival at a given location may be detected in different ways, depending on the technique used to investigate jet penetration. It may be defined by the first tracer crossing the LDV measuring volume positioned at a certain location or the first cluster of particles or by the detection of a certain concentration of injected gas, and so on. In the present investigation, two-dimensional images of the seeded jet, obtained by two-dimensional laser sheet visualization at different times ASI, were processed to measure the tip position. The images were preprocessed by subtracting the background, obtained from a picture taken without the jet, and then the negative images were computed. At any given axial position, the average gray level I_{av} of the image along a line perpendicular to the jet axis (Fig. 3a) was evaluated as

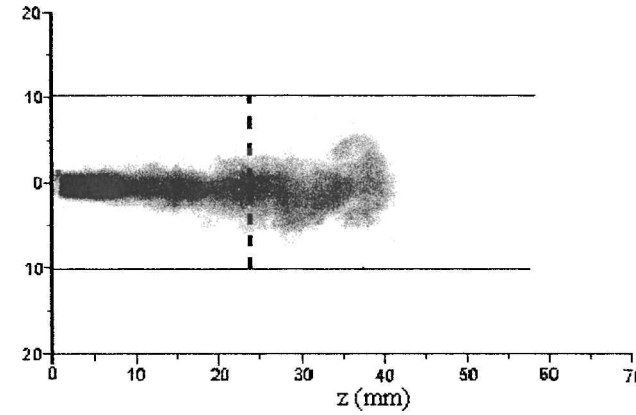

a)

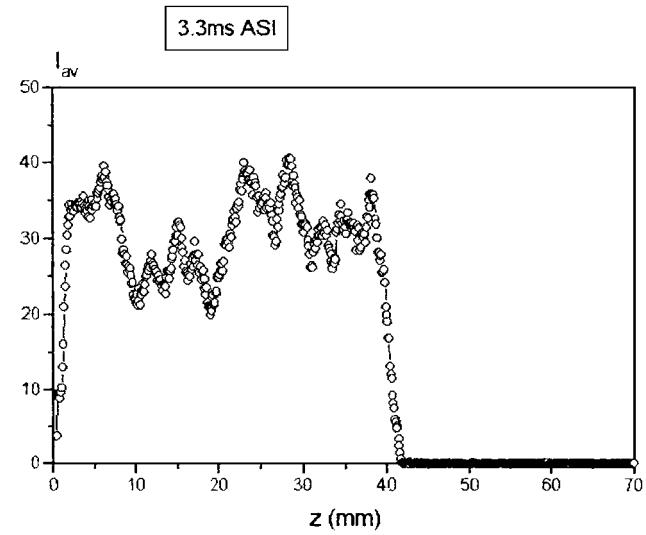

b)

Fig. 3 Evaluation of the a) average gray level from the two-dimensional image and b) average gray level $I_{av}(z)$ at any distance from the nozzle.

$$I_{av}(z) = \int_{-r_1}^{+r_1} I(r, z)\, dr \Big/ 2r_1$$

where $I(r, z)$ is the gray level at position (r, z), which obtains for each image a distribution of the average gray level as a function of nozzle distance only (Fig. 3b). Then, by setting a threshold level and evaluating the farthest distance from the nozzle tip at which the threshold is reached, it is possible to define the tip position. The results will depend on the chosen threshold level, but Fig. 4 indicates how this influence is small when care is taken to obtain well-contrasted pictures. Based on the scatter of data relative to pictures taken at the same time ASI, the uncertainty of each measurement was a result of the order of the picture spatial accuracy (0.3 mm) close to the nozzle, increasing up to 1.8 mm when the tip reaches 60 mm. The measurements at the farthest location, about 72 mm, show large scattering ($\approx$7 mm) because jet dilution by the surrounding air decreases the picture contrast.

A recent paper[10] reports a comprehensive analysis of experimental data on transient gas jets. Assuming self-similarity of the velocity profiles, it was shown that the variable $\eta = z/(J/\rho)^{1/4}$ depends linearly on $t^{1/2}$ with a slope equal to 3 ± 0.1, that is, $\eta = 3t^{1/2}$. Plotting the present results as η vs $t^{1/2}$ (see Fig. 5), it can be seen how the rule holds approximately only for downstream distances greater than six nozzle diameters.

Observation of the pictures and further image processing provided information about the internal structure of the unsteady jet. Figure 6b shows the gray level distribution (representing the light intensity distribution) of the image in Fig. 6a. As in other similar images, a fluttering of the growing jet is visible, a phenomenon that can be

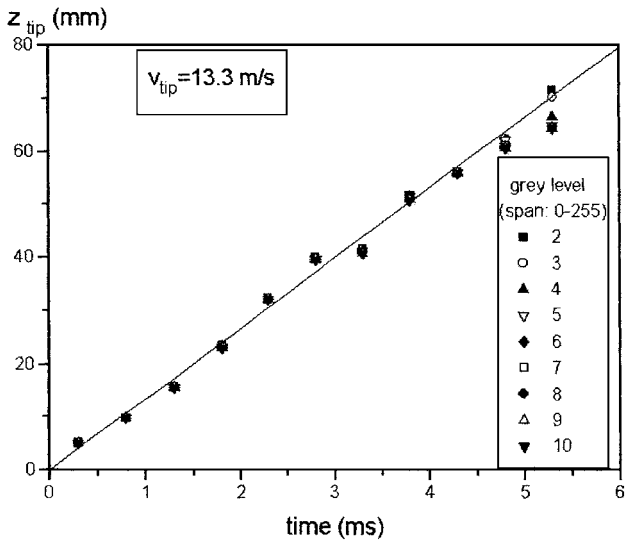

Fig. 4 Jet tip penetration from two-dimensional images; reported average tip velocity was obtained by linear fitting.

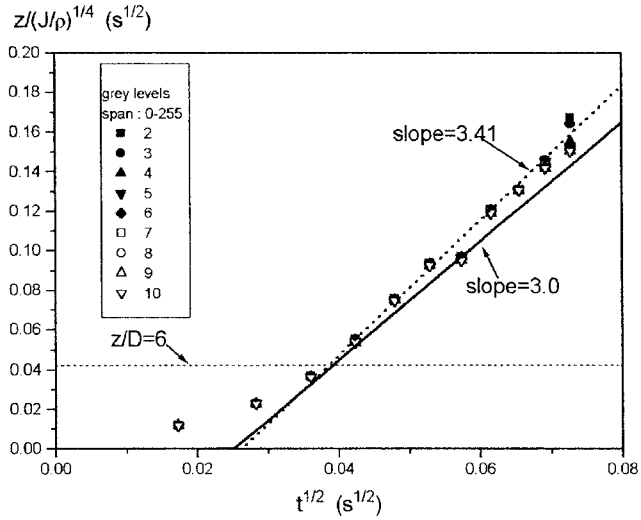

Fig. 5 Jet penetration from two-dimensional images plotted using the variables suggested in Ref. 10: ----, linear fitting of points relative to distances larger than six nozzle diameters.

considered responsible for the formation of the irregular head edges and subsequent entrainment of surrounding air. To quantitatively appreciate the phenomenon, the jet center of mass was evaluated, for each picture, as

$$r_{\mathrm{cm}}(z) = \frac{\int_{-r_1}^{+r_1} r I(r, z)\, \mathrm{d}r}{\int_{-r_1}^{+r_1} I(r, z)\, \mathrm{d}r}$$

The function $r_{\mathrm{cm}}(z)$ gives the profile of the center of mass of the two-dimensional picture of the jet, and Fig. 7 shows how it fluctuates while the jet is developing. Obviously it was impossible to correlate quantitatively such fluctuations to air entrainment; however, a further image analysis allowed to evaluate the total jet volume, which gives information about entrainment. When a threshold for the gray level is set, the jet contour can be defined and the local diameter (L in Fig. 8a) evaluated; then the jet volume has been estimated as the volume obtained summing up all of the disks with diameter $L(z)$ and thickness $\mathrm{d}z$, that is,

$$V = \frac{\pi}{4} \int_0^{z_{\mathrm{tip}}} L^2(z)\, \mathrm{d}z$$

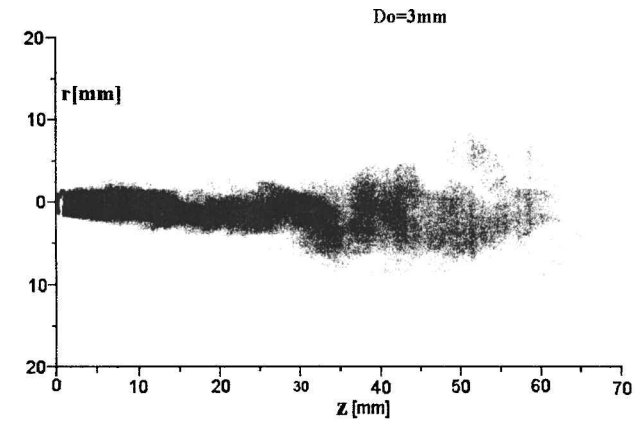

Fig. 6a Two-dimensional image of the jet at $t = 4.8$ ms ASI.

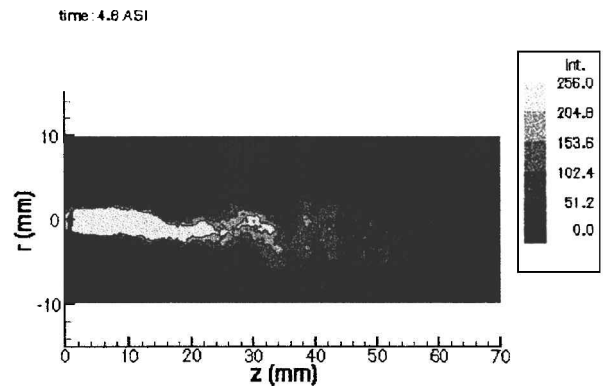

Fig. 6b Scattered light intensity (in gray scale levels) from Fig. 6a image.

This extension of a two-dimensional image into a three-dimensional one involves errors, which cannot be estimated. The CCD camera resolution introduces errors in evaluating this volume that were estimated between 5 and 8%. Figure 8b shows the jet volume as a function of time. When the data are fitted and extrapolation is made at $t = 0$, the injected volume flow rate at the beginning of injection was deduced: $\dot{V} = 2 \times 10^{-4}$ m^3/s. The associated mean injection velocity resulted: $v_0 = 28.3$ m/s. This value should be compared with the injection velocity, evaluated from the injection pressure trace at the beginning of injection, which is equal to 69 m/s. From the injection pressure, it was also possible to evaluate the injected gas volume as a function of time, under the hypothesis of quasi-steady-state conditions. The result is shown in Fig. 8b (dotted line), and it is expected to be an upper limit of the actual instantaneous injected volume. It is interesting to compare the measured jet volume to the estimated injected volume. That after 3 ms ASI the jet volume becomes larger than the upper limit of the injected volume seems to indicate that the jet head actually entrains surrounding air, a result that cannot be deduced from the measured velocity field, as will be shown later.

B. LDV Results

LDV measurements of air velocity were collected over many subsequent injections and ensemble averaged over time slots 0.25 ms wide. The axial velocity on the jet axis, U_c, was evaluated as the average taken over the region $-1 \le r \le +1$ mm, to account for asymmetry of the measurements (the rms of the averaged values varied from 1 up to 10% of U_c, depending on time and position). U_c is plotted vs time in Fig. 9 for each of the five axial locations at which complete velocity profiles were measured by LDV, that is, 30, 40, 50, 60, and 65 mm. When a velocity threshold $v_{z,\mathrm{th}}$ was set, it was possible to define the instant at which the threshold is crossed at each location as the time arrival of the jet tip. The estimated velocity accuracy can be translated into accuracy of jet tip penetration

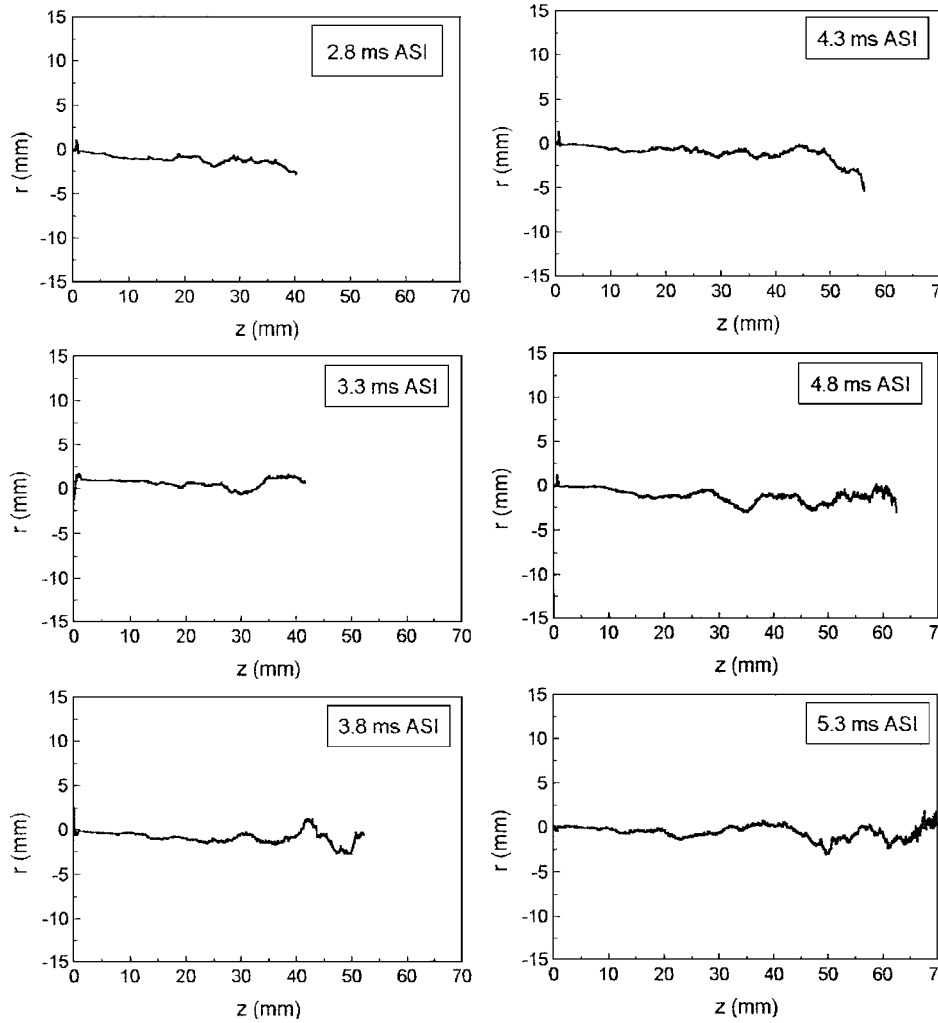

Fig. 7 Jet center of mass for a set of two-dimensional images, at different times after injection.

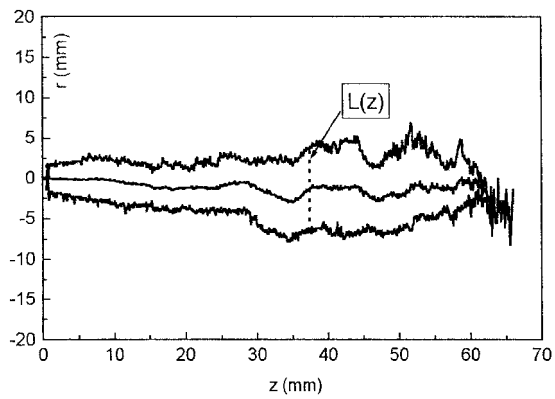

Fig. 8a Jet contour and local width $L(z)$ from two-dimensional images ($t = 4.8$ ms ASI).

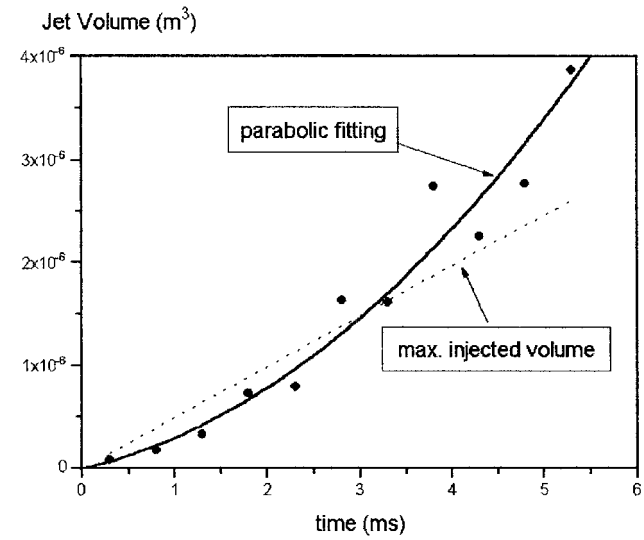

Fig. 8b Jet volume calculated from two-dimensional images.

measured by LDV by evaluating the steepness of the centerline axial velocity curves in Fig. 9. The accuracy of the tip arrival time is between 0.02 and 0.044 ms, which can be translated into spatial accuracy ranging from about 0.3 to 0.6 mm.

Figure 10 shows the results obtained by taking $v_{z,t} = 2$ m/s. It can be easily recognized that those points do not represent the actual tip penetration, as measured from two-dimensional visualization. It was possible to reobtain the values measured from the pictures only setting the velocity threshold at about 70% of the maximum axial velocity reached at that location (Fig. 10). This result may be interpreted as follows: The ambient air starts to move before the actual jet tip arrives at the location as it is pushed away by the jet head. The delay between the beginning of air movement and the arrival of the jet tip is about 0.85 ms, which means that the influence of the jet head is felt by the ambient air at a distance of about 10–12 mm ($\approx 3.5 D_0$) ahead of the jet head. Note that this result agrees with Ref. 10 and also that Witze[13] defined the arrival time of the jet tip as the instant when the average velocity reached 70% of the final steady-state value, following a procedure already introduced by Abramovich and Solan.[14]

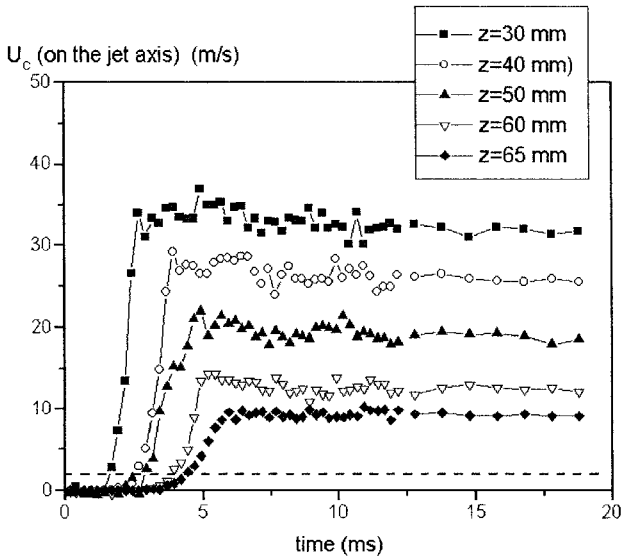

Fig. 9 Axial velocity on the jet axis, U_c vs time ASI, at different distances from the nozzle.

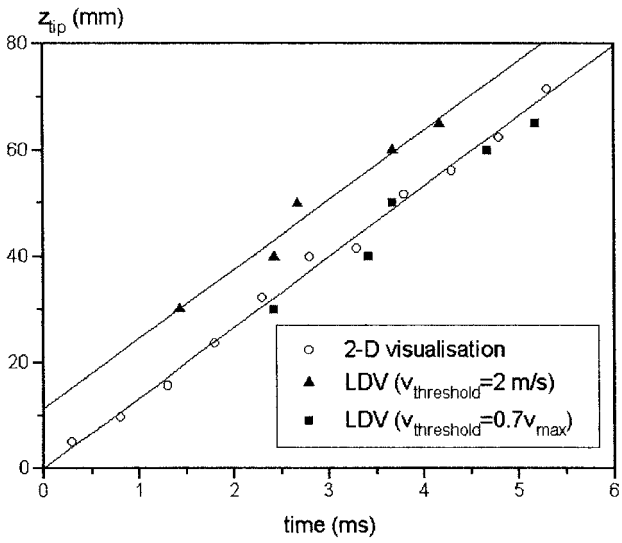

Fig. 10 Tip penetration from two-dimensional visualizations and from LDV measurements with two different threshold levels.

Figure 11 shows the centerline velocity, nondimensionalized by the jet centerline velocity at the same position under steady-state conditions $[v_c = U_c(z, t)/U_{c,\text{steady}}(z)]$ vs the nondimensional time defined as $\tau = (t - t_{\text{tip}})/t_{\text{tip}}$, where t_{tip} is the tip arrival time at the given location. After this nondimensionalization, the experimental points relative to the initial ramps collapse together, following an unique law of the form $v_c = v_c(\tau)$.

After the arrival of the tip at a given location, the centerline axial velocity U_c reaches its maximum value in a time ranging from about 1 to 2 ms (depending on the distance from the nozzle), then the axial velocity decreases slightly to reach its steady-state value. This quick attainment of an almost steady-state condition on the jet axis does not mean that the actual steady-state jet structure is reached. To better show this point, the axial component of the measured air velocity, $v_z(z, r, t)$, was first nondimensionalized as

$$\alpha(z, r, t) = \frac{|v_z(z, r, t) - v_{z,\text{steady}}(z, r)|}{U_c(z)}$$

where $v_{z,\text{steady}}(z, r)$ is the value of v_z at location (z, r) when steady regime is reached and $U_c(z) = v_{z,\text{steady}}(z, 0)$ is the steady-state centerline velocity. The approach of $\alpha(z, r, t)$ to zero quantifies the approach to the steady state.

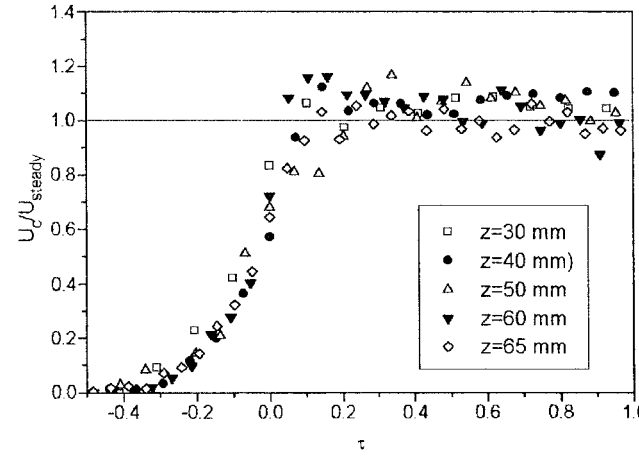

Fig. 11 Centerline axial velocity nondimensionalized by the centerline axial steady velocity as a function of the nondimensional time: $\tau = (t - t_{\text{tip}})/t_{\text{tip}}$.

Figure 12 shows maps of α at different times ASI, and it is possible to see how the approach to steady conditions is faster on the axis than on the borders. This is because the jet inner structure in the near field is dominated by the inertia of the flow injected through the nozzle. Whereas at the jet edges, the structure is mainly dominated by the injected/surrounding gas interaction through momentum and mass transfer in radial direction, and this phenomenon needs longer times to reach steady-state conditions. It is actually the latter phenomenon that is responsible for the entrainment of surrounding air. Also, entrainment needs more time to reach steady-state conditions, as will be shown.

The radial velocity measured along two opposite lines parallel to the jet axis was used to evaluate air entrainment, using the same method adopted in previous investigations.[20–22] A cylindrical control surface enclosing the jet was subdivided into many rings (Fig. 2) and the air mass flow rate entering through any ring (partial entrained mass flow rate) was estimated from the measured radial velocity

$$\dot{m}_{p,e} = \int_{\text{ring}-p} \rho_e v_r(z, R, t)\, \mathrm{d}S$$

The radial velocities at each measurement location were considered representative of the air velocity relative to a half-ring (Fig. 2). The total entrained air mass flow rate crossing any section of the cylinder normal to its axis can then be evaluated by summing up all of the partial entrained mass flow rates from the top plate ($z = 0$) to the actual cross section position.

The choice of the radius of the cylindrical surface is critical. A small radius is expected to reduce the relative error in the measured velocity because the radial velocity increases going toward the axis during the entrainment process. On the other hand, near the jet edge, the measurement of the entrainment velocity becomes less accurate due to the interference with the jet turbulent boundaries and the existence of a significant axial velocity component. Tests were carried out to optimize the choice. The radial velocity was measured under steady-state conditions at different distances from nozzle and radial locations. When the rms velocity vs radial position was plotted, a sharp increase was evidenced when the measurement location was moved through the jet borders. The optimal distance, $R = 20$ mm, was chosen as the closest location to the jet axis were the rms velocity was still comparable to that found at larger distances.

From the theory of steady turbulent jets and the experimental results of Ricou and Spalding,[23] it is possible to show that the entrainment coefficient

$$K'_e = \frac{\mathrm{d}\dot{m}_e}{\mathrm{d}z}\left(\frac{D_0}{\dot{m}_0}\right)\left(\frac{\rho_0}{\rho_e}\right)^{\frac{1}{2}}$$

assumes a constant value (=0.32) in the jet far field, that is, $z > 10D_0$ (also see Ref. 24). The existence of such a universal constant comes

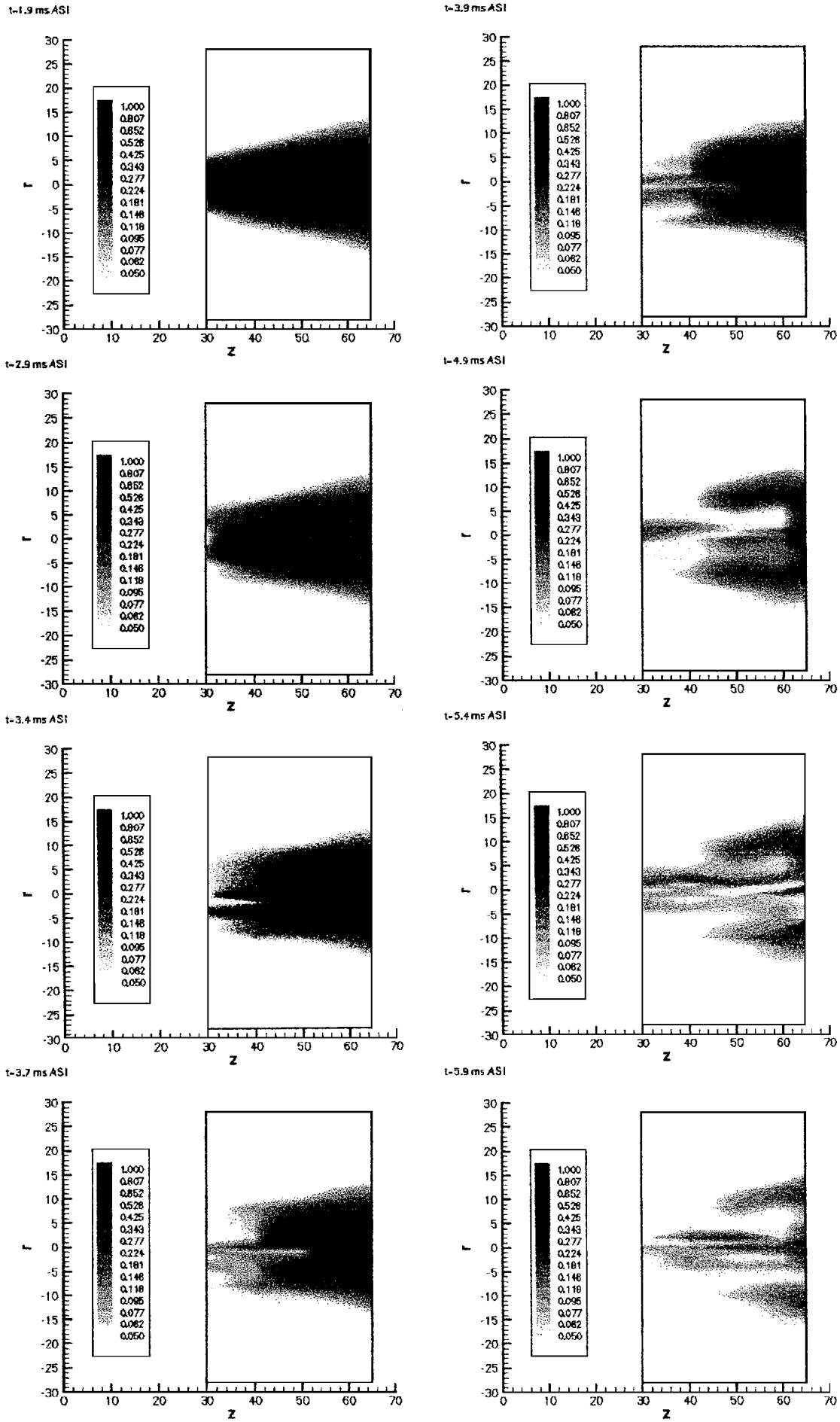

Fig. 12 Two-dimensional imaging of α at different times ASI.

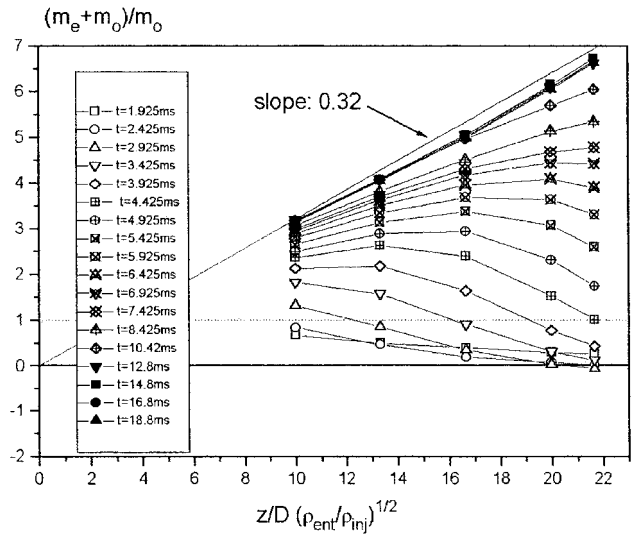

Fig. 13 Nondimensional jet mass flow rate θ vs nondimensional distance ξ for different times ASI.

from self-similarity of velocity profiles across the jet. For the unsteady jet, K_e' is not a constant, due to both the unsteadiness of the flow and the non-self-similarity of the velocity profiles. However, it is interesting to analyze the value of the nondimensional parameter

$$\mu = (\dot{m}_e + \dot{m}_0)/\dot{m}_0$$

vs the nondimensional nozzle distance $\xi = z/D_0(\rho_e/\rho_0)^{1/2}$, which for a steady turbulent jet would be $\mu = 0.32\xi$. As expected, the parameter μ shows a nonlinear dependence on ξ, which changes with time but tends to the asymptotic behavior described earlier at a relatively long time (Fig. 13). The average slope of the quasi-steady-state measurements is 0.301, 6% lower than the far-field value, which shows again that, also for the entrainment process, steady-state conditions are not reached suddenly.

C. Discussion

The observation of the whole velocity field around the jet head (Fig. 14a) shows the existence of a recirculation zone: a toroidal vortex surrounding the jet head. This confirms that entrainment of surrounding air (similar to steady jets, see Fig. 14c) is not yet established and that a transition period exists between the passage of the vortex and the attainment of steady entrainment (Fig. 14b). The radial velocity component measured at different distances from the jet axis and axial locations always shows the typical time history as shown in Fig. 15, a negative (outward directed) peak followed by a quick approach to the steady-state value. The negative peak in radial velocity is due to the air pushed apart by the jet head passing by the measurement location, and the peak increases as the measurement location moves toward the jet axis. Then the radial velocity reaches a positive (inward directed) steady value, when the jet head has moved away, and this steady value increases as measurement location moves toward the jet axis. The steadiness of the radial velocity at locations external to the jet cone characterises the steady-state entrainment flowfield (see also Fig. 14c), and mass conservation is responsible for velocity increase while moving toward the jet axis.

The zero crossing of the radial velocity was used (similar to that in Refs. 21 and 25) to define the location of jet head center. Data taken at different radial positions show that the time at which the radial velocity changes sign is different and increases as the radial coordinate increases. Figure 16 shows the axial coordinate of the radial velocity zero crossing as a function of time for different radial locations (from 8 to 20 mm). It is possible to estimate the velocity at which this toroidal vortex moves downstream, finding different values (from 8.8 to 10.6 m/s) at different radial positions. It is more difficult to define the time at which a steady value of the radial

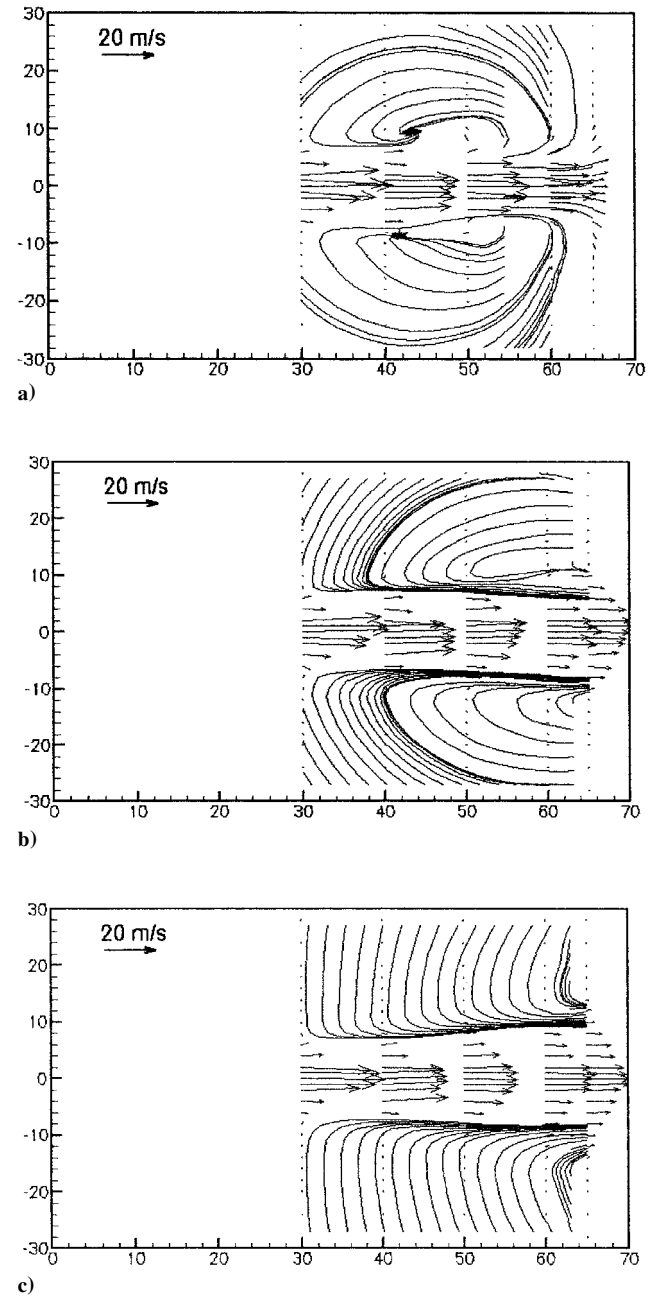

Fig. 14 Velocity flowfield a) inside and outside the jet (at $t = 4.8$ ms ASI), b) inside and outside the jet (at $t = 6.5$ ms ASI), and c) under steady conditions.

velocity is reached. However, when a threshold of 80% of the steady-state radial velocity value (Fig. 17a) is chosen, it is possible to separate the steady jet region from the unsteady region, at least for radial locations outside the main jet cone. The results of this calculation for $r = 16$ and 20 mm are shown in Fig. 17b.

It is then clear that a zone exists, behind the jet tip, were the gas jet structure is different from that of the quasi-steady jet. Under the present conditions, the dimension of this region can be estimated as the distance from the jet tip and the beginning of the quasi-steady jet region as just defined. Figure 17b shows that the dimension of the jet head is larger than $12D_0$ in the near-field region investigated, and it is growing linearly with time.

When the velocity flowfield in Fig. 14 is observed, it can be seen that there exists a zone around the jet head, delimited by the cylinder of radius 20 mm, where the recirculation caused by the head movement produces air entrainment into the following steady-state jet. This entrainment cannot be detected by the integration of the radial velocity along the cylindrical surface. From the earlier analysis of the flowfield, the jet head appears to be, on one hand,

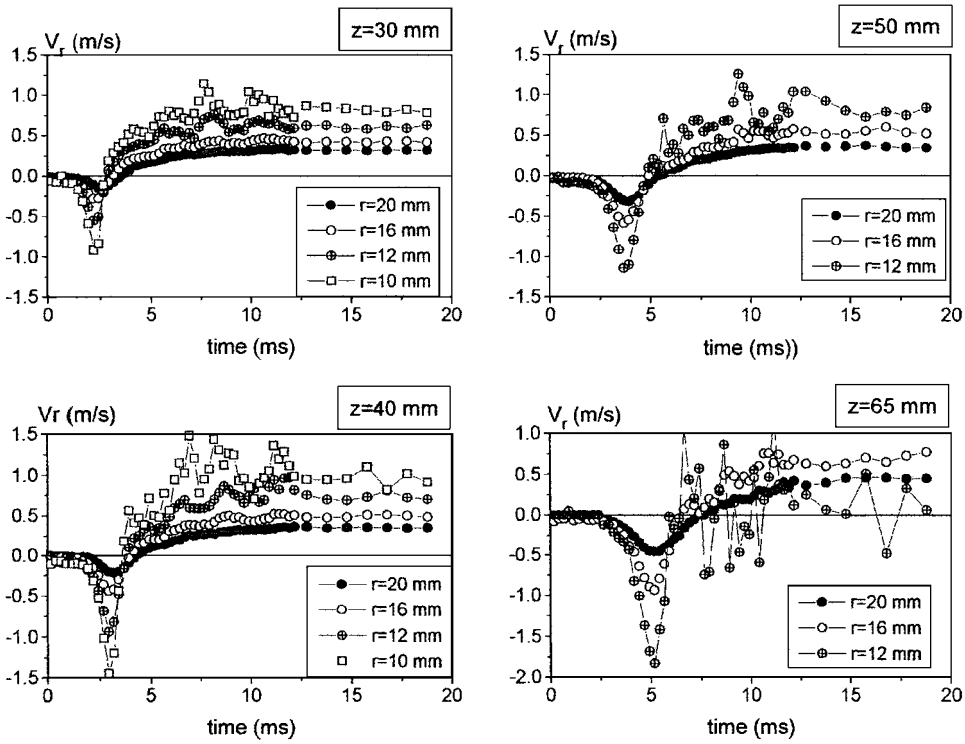

Fig. 15 Radial velocity components vs time ASI at different axial and radial positions.

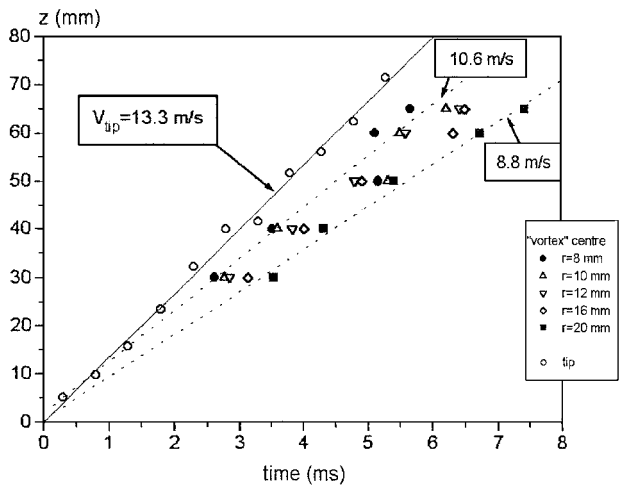

Fig. 16 Tip and vortex center penetration.

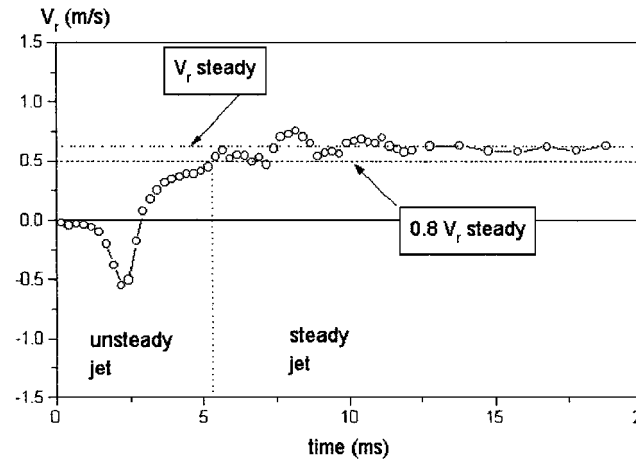

Fig. 17a Threshold level for the definition of the jet head size.

a region of high mixing, whereas, on the other hand, it is a rather compact structure that pushes the ambient gas apart, apparently producing low direct mixing with the surroundings.

Indeed, the widely used model proposed in Refs. 13 and 14 gives acceptable results in evaluating tip penetration,[10] particularly for the far-field region. This seems to be in contrast with the earlier mentioned capability of the jet head to entrain air directly by the surroundings because the model assumes no direct entrainment by the jet head (also see Ref. 10, where a quite general penetration law was obtained under the same hypotheses). A way to resolve the ambiguity is the following. When the tip is sufficiently far from the nozzle, the quasi-steady jet entrains air through the cone boundaries in a quantity roughly proportional to its length. This quantity may become much larger than that directly entrained by the jet head, leading to correctness of the model assumption. However, when the tip is close to the nozzle, the steady-state jet region practically does not exist, and entrainment is only possible by direct interaction of jet head with surrounding air, leading to failure of the model hypothesis.

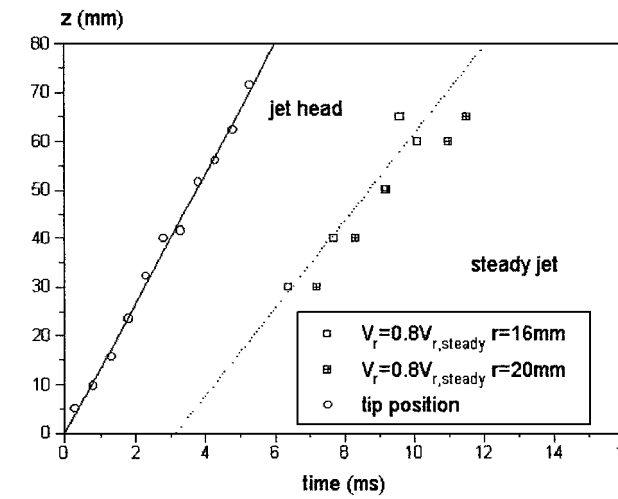

Fig. 17b Jet head and steady jet regions.

V. Conclusions

The flow characteristics of an impulsively started gas jet were analyzed in the near-field region by two-dimensional imaging and measurement of the two-dimensional velocity field inside and outside the jet. The analysis of the results yields the following conclusions about the inner and outer structure of such a jet.

1) The techniques used for tip penetration measurements, namely, laser sheet visualization and LDV, allowed definition of a region in front of the jet head where the air is pushed ahead by the incoming jet, and the thickness of this region was found about $3.5D_0$.

2) Image analysis allowed an estimate of the jet volume. Comparison of the increasing rate of the jet volume to the injected volume flow rate suggests that entrainment of surrounding air by the jet head also may take place at the beginning of the injection. However, the measured air flowfield around the jet suggests that such entrainment has a cause very different from the entrainment into steady jets: It is likely to be due to the large wrinkling of the jet border caused by fluttering of the jet that traps surrounding air into the head.

3) LDV measurements of the gas flowfield around and inside the jet head provided the value of the entrained mass flow rate and from these quantitative results it is possible to show the following. a) The jet mass flow rate reaches the quasi-steady value with a delay, after tip arrival, which depends on the distance from the nozzle. b) The flowfield around the jet tip shows the presence of a region of strong recirculation that renders the entrainment characteristics of this region to be very different from those of the quasi-steady-state jet. c) The length of the jet head was estimated to be larger than $12D_0$ and grows linearly with time in the region analyzed.

4) The flow on the jet axis attains quasi-steady conditions very rapidly, whereas jet borders need more time to reach a steady structure. This behavior is due to the jet axis flow in the near field being dominated by inertia effects of the injected gas, whereas the jet border structure being dominated by turbulent diffusion of mass and momentum, which have larger characteristic times.

Acknowledgments

The experimental work has been carried out at the laboratories of the Istituto per la Tecnologia dei Materiali e dei Processi Energetici of the Italian National Research Council (TEMPE-CNR) (previously CNPM-CNR). The authors would like to thank G. Brunello for valuable cooperation concerning data acquisition and processing.

References

[1]Wygnanski, I., and Fiedler, H., "Some Measurements in the Self-Preserving Jet," *Journal of Fluid Mechanics*, Vol. 38, Pt. 3, 1969, pp. 577–612.

[2]Hussein, H. J., Capp, S. P., and George, W. K., "Velocity Measurements in High Reynolds Number, Momentum Conserving, Axisymmetric, Turbulent Jet," *Journal of Fluid Mechanics*, Vol. 258, 1994, pp. 31–75.

[3]Schlichting, H., *Boundary Layer Theory*, McGraw–Hill, New York, 1979, Chap. 24.

[4]Schetz, J. A., *Injection and Mixing in Turbulent Flow*, edited by M. Summerfield, Vol. 68, Progress in Astronautics and Aeronautics, AIAA, New York, 1980, Chap. 8.

[5]Rubas, P. J., Paul, M. A., Martin, G. C., Coverdill, R. E., Lucht, R. P., Peters, J. E., and Del Vecchio, K. A., "Methane Jet Penetration in a Direct-Injection Natural Gas Engine," Society of Automotive Engineers, SAE Paper 980143, Feb. 1998.

[6]Hill, W. G., and Greene, P. R., "Increased Turbulent Jet Mixing Rates Obtained by Self-Excited Acoustic Oscillations," *Journal of Fluids Engineering*, Vol. 99, 1977, pp. 520–525.

[7]Bremhorst, K., and Watson, R. D., "Velocity Field and Entrainment of a Pulsed Core Jet," *Journal of Fluids Engineering*, Vol. 103, 1981, pp. 605–608.

[8]Bremhorst, K., and Hollis, P. G., "Velocity Field of an Axisymmetric Pulsed, Subsonic Air Jet with a Significant No Flow Period Between Pulses," *AIAA Journal*, Vol. 28, 1990, pp. 2043–2049.

[9]Randolph, H., Chew, L., and Johari, H., "Pulsed Jets in Supersonic Crossflow," *Journal of Propulsion*, Vol. 10, No. 5, 1994, pp. 746–748.

[10]Hill, P. G., and Ouellette, P., "Transient Turbulent Gaseous Fuel Jets for Diesel Engines," *Journal of Fluids Engineering*, Vol. 121, 1999, pp. 93–101.

[11]Birch, A. D., Brown, D. R., Dodson, M. G., and Swaffield, F., "The Structure and Concentration Decay of High Pressure Jets of Natural Gas," *Combustion Science and Technology*, Vol. 36, 1984, pp. 249–261.

[12]Turner, J. S., "The Starting Plume in Neutral Surroundings," *Journal of Fluid Mechanics*, Vol. 13, Pt. 3, 1962, pp. 356–368.

[13]Witze, P. O., "The Impulsively Started Incompressible Turbulent Jet," Sandia Labs., Rept. SAND80-8617, Livermore, CA, Oct. 1980.

[14]Abramovich, S., and Solan, A., "The Initial Development of a Submerged Laminar Round Jet," *Journal of Fluid Mechanics*, Vol. 59, Pt. 4, 1973, pp. 791–801.

[15]Kuo, T. W., and Bracco, F. V., "On the Scaling of Transient Laminar, Turbulent and Spray Jets," Society of Automotive Engineers, SAE Paper 820038, Feb. 1982.

[16]Hay, N., and Jones, P. L., "Comparison of the Various Correlations for Spray Penetration," Society of Automotive Engineers, SAE Paper 720776, Sept. 1972.

[17]Wan, Y., and Peters, N., "Scaling of Spray Penetration with Evaporation," *Atomization and Sprays*, Vol. 9, 1999, pp. 111–132.

[18]Hyun, G. -S., Nogami, M., Hosoyama, K., Senda, J., and Fujimoto, H., "Flow Characteristics in Transient Gas Jets," Society of Automotive Engineers, SAE Paper 950847, Feb.–March 1995.

[19]Kido, A., Ogawa, H., and Miyamoto, N., "Quantitative Measurements and Analysis of Ambient Gas Entrainment into Intermittent Gas Jets by Laser-Induced Fluorescence of Ambient Gas (LIFA)," Society of Automotive Engineers, SAE Paper 930970, March 1993.

[20]Cossali, G. E., Brunello, G., and Coghe, A., "LDV Characterisation of Air Entrainment in Transient Diesel Sprays," Society of Automotive Engineers, SAE Paper 910178, Feb.–March 1991.

[21]Andriani, R., Coghe, A., and Cossali, G. E., "Near Field Entrainment in Gas Jets and Diesel Sprays: A Comparative Study," *Twenty-Sixth (International) Combustion Symposium*, Combustion Inst., Pittsburgh, PA, 1996, pp. 2549–2556.

[22]Cossali, G. E., Coghe, A., Gerla, A., and Brunello, G., "Effect of Gas Temperature and Density on Air Entrainment in Transient Diesel Sprays," Society of Automotive Engineers, SAE Paper 960862, Feb. 1996.

[23]Ricou, F. P., and Spalding, D. B., "Measurements of Entrainment by Axisymmetrical Turbulent Jets," *Journal of Fluid Mechanics*, Vol. 11, Pt. 1, 1961, pp. 21–32.

[24]Hill, B. J., "Measurement of Local Entrainment Rate in the Initial Region of Axisymmetric Turbulent Air Jets," *Journal of Fluid Mechanics*, Vol. 51, Pt. 4, 1972, pp. 773–779.

[25]Coghe, A., Cossali, G. E., Crespi, G. M., and Sanchez Simon, M. L., "An Unconventional Application of Phase Doppler Anemometry for Coherent Structure Reconstruction of Two Phase Unsteady Flow," *Experimental and Numerical Flow Visualization*, Fluid Engineering Div. Vol. 172, American Society of Mechanical Engineers, Fairfield, NJ, 1993, pp. 29–34.

P. R. Bandyopadhyay
Associate Editor